ACS APPLIED MATERIALS & INTERFACES

Research Article

www.acsami.org

Confine Clay in an Alternating Multilayered Structure through Injection Molding: A Simple and Efficient Route to Improve Barrier Performance of Polymeric Materials

Feilong Yu, Hua Deng,* Hongwei Bai, Qin Zhang, Ke Wang, Feng Chen, and Qiang Fu*

College of Polymer Science and Engineering, State Key Laboratory of Polymer Materials Engineering, Sichuan University, Chengdu 610065, China

Supporting Information

ABSTRACT: Various methods have been devoted to trigger the formation of multilayered structure for wide range of applications. These methods are often complicated with low production efficiency or require complex equipment. Herein, we demonstrate a simple and efficient method for the fabrication of polymeric sheets containing multilayered structure with enhanced barrier property through high speed thin-wall injection molding (HSIM). To achieve this, montmorillonite (MMT) is added into PE first, then blended with PP to fabricate PE-MMT/PP ternary composites. It is demonstrated that alternating multilayer structure could be obtained in the ternary composites because of low interfacial tension and good viscosity match between different polymer components. MMT is selectively dispersed in PE phase with partial exfoliated/partial intercalated microstructure. 2D-WAXD analysis indicates that the clay tactoids in PE-MMT/PP exhibits an uniplanar-axial orientation with their surface parallel to the molded part surface, while the tactoids in binary PE-MMT composites with the same overall MMT contents illustrate less orientation. The enhanced orientation of nanoclay in PE-MMT/PP could be attributed to the confinement of alternating multilayer structure, which prohibits the tumbling and rotation of nanoplatelets. Therefore, the oxygen barrier property of PE-MMT/PP is superior to that of PE-MMT because of increased gas permeation pathway. Comparing with the results obtained for PE based composites in literature, outstanding barrier property performance (45.7% and 58.2% improvement with 1.5 and 2.5 wt % MMT content, respectively) is achieved in current study. Two issues are considered responsible for such improvement: enhanced MMT orientation caused by the confinement in layered structure, and higher local density of MMT in layered structure induced denser assembly. Finally, enhancement in barrier property by confining impermeable filler into alternating multilayer structure through such simple and efficient method could provide a novel route toward high-performance packaging materials and other functional materials require layered structure.

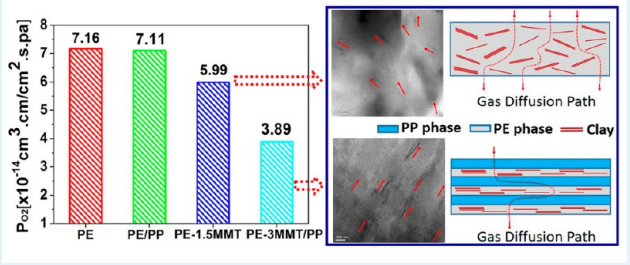

KEYWORDS: *multilayered structure, clay, orientation, barrier, high speed thin wall injection molding*

1. INTRODUCTION

The construction of multilayered structure has been widely investigated to prepare biomimic and high performance functional materials.[1,2] It is thought that the formation of alternating layered structure is able to confine filler or polymer into the structure to enhance various properties, including mechanical properties, barrier properties, etc.[3−6] A number of methods have been reported to achieve this. For instance, the use of layer multiplying coextrusion enables the fabrication of layered sheets with tens to thousands of alternating layers of two or three different polymers with individual layer thicknesses between 10 nm and 100 μm. This technique is beneficial for creating laminar morphology with high aspect ratio. As a consequence, the increased gas diffusion pathway could result in significant barrier property enhancement.[7] Furthermore, as the layer thickness approaches nanometer scale, the change in crystal superstructure and lamellae arrangement for semicrystalline polymers also play vital role for improving barrier property. Wang et al. has utilized layer-multiplying coextrusion process to obtain the assembly of alternating nonolayers of poly(ethylene oxide) (PEO) and poly(ethylene-*co*-acrylic acid) (EAA). While the confinement is near lamellar thickness size, PEO layers crystallize as single, high-aspect-ratio lamellae that resemble single crystals parallel to the nanolayer. This leads to 2 orders of magnitude reduction in gas permeability compared with spherulitic PEO crystal superstructure.[8] Moreover, efforts have been made to create designed architecture in particle-filled polymers such as alternating filled/unfilled layers to improve barrier property via such layer multiplying coextrusion technique.[9−11] Furthermore, Yu et al. have prepared oriented layer-like microstructure comprised of oriented polymer sheet and deformed

Received: January 12, 2015
Accepted: April 27, 2015
Published: April 27, 2015

DOI: 10.1021/acsami.5b00347
ACS Appl. Mater. Interfaces 2015, 7, 10178−10189

particles via so-called pressure-induced flow (PIF) processing.[12] Meanwhile, layer by layer (LbL) deposition process has been proposed as a facile technique to construct alternating layered structure, which leads to nanoplatelets well aligned perpendicular to the gas diffusion direction and thus obtaining markedly enhanced barrier property.[13,14] Walther et al. have also prepared highly aligned hard/soft layered composites in a water-based processing approach akin to paper-making.[15,16] Other strategies, such as uncontrolled casting of polymer/clay mixtures,[17,18] ice-templating and sintering of ceramics,[19,20] electrodeposition technology induced assembly of nanoplatelets,[21] and the evaporation-induced partitioning and self-assembly method[22] have also been reported to prepare polymer-based nanocomposites with layered like structure aiming to achieve notable enhancement in various properties.

Regarding barrier properties, it is widely believed that the key for fabrication of polymer sheets with superior barrier property is to orient impermeable materials perpendicularly to the gas diffusion direction.[23−25] Thus, constructing multilayered structure containing impermeable materials is thought as an important route. However, above-discussed methods are complicated processes with quite low production efficiency or require complicated equipment, which limits their large-scale industrial application. Therefore, it is of crucial importance to find a simple and efficient method to fabricate polymer sheets containing multilayered structure with superior barrier property.

Injection molding provides the possibility to efficiently fabricate sheets for packaging applications due to its high production efficiency, full automation, excellent dimension control, as well as simple fabrication process. However, conventional injection molding process could not fulfill the requirement for the fabrication of thin-wall sheets in consideration of several drawbacks. For example, the insufficient injection pressure and injection speed is not adequate for the melt fully filling into mold cavity because of increased flow resistance caused by thin-wall mold. In recent years, high speed thin-wall injection molding (HSIM) is considered as a promising strategy for packaging sheet fabrication due to its high injection speed and intense flow field.[26,27] Such characteristics of HSIM provide opportunity to obtain special blend morphologies which could be beneficial for improving barrier property. For polymer composites, HSIM can not only provide short production cycle, but also provide extra shear and confinement to the system, which could induce more orientation in polymer chains as well as fillers. It might also affect the viscosity, as well as chain entanglement, and thus processing ability. These issues might play important role for the final properties of polymer composites. In our previous work, a multilayered structure with alternating layers of isotactic polypropylene (iPP) and high density polyethylene (HDPE) were prepared through injection molding HDPE/PP blends into thin-wall mold.[28] It is thought that the intense flow field, small interfacial tension and viscosity ratio between polymer blends compositions play important role on the formation of such structure. In current study, to confine impermeable filler into such layered structure for barrier properties, MMT is added into PE first, and blended with PP subsequently. These blends are injection molded by HSIM with the hope to confine MMT in PE phase to enhance their orientation. To understand the structure−property relationship, systematic study has been performed to investigate issues such as phase morphology, barrier property, polymer crystallinity, as well as orientation degree of clay, etc.

2. EXPERIMENTAL SECTION

2.1. Materials. The HDPE supplied by Fushun Petro-chemical Corp (2911) has a melt flow index of 20 g/10 min (2.16 kg, 190 °C) and density of 0.96 g/cm^3. Commercially available iPP (T30S) with a melt flow index of 2.6 g/10 min (2.16 kg, 230 °C) and density of 0.91 g/cm^3 was provided by Lanzhou Petrochemical Corp. The clay used in this study was a commercial organoclay supplied by Nanocor Corp (Nanomer I.44P), Nanomer I.44P is a dimethyl, dihydrogenated tallow ammonium salt modified montmorillonite (org-MMT), the interlayer spacing of (001) plane and organic content is in the range of 24−26 Å and 36−40 wt %, respectively. Maleic anhydride grafted PE (trademarked as C-26) used as compatibilizer was purchased from Westlake Chemical Corp. C-26 has an acid number of 8 mg KOH/g and molecular weight Mw of 65 000 according to the supplier.

2.2. Sample Preparation. First, MMT was blended with PE to prepare masterbatch consisting of 10 wt % clay and 30 wt % C-26 in twin screw extruder with temperature in the range of 140−200 °C from hopper to die. After that, the masterbatch was further diluted into binary PE-MMT composites with different clay contents using twin screw extruder, respectively. Subsequently, single screw extruder was utilized to blend PP with PE-MMT pellets at weight proportion 5:5 to fabricate ternary PE-MMT/PP composites. Possible migration of clay to PP phase is hindered because of its relative weak shear. The obtained PE-MMT/PP pellets were then subjected to HSIM at an injection speed of 600 mm/s and a melt temperature of 200 °C to obtain PE-MMT/PP naocomposite sheets with the size of 80 mm × 60 mm and a thickness of 0.4 mm. The detailed schematic diagram of injection molded specimen is shown in Figure 1. The as-obtained PE-MMT/PP nanocomposites are labeled as PE-xMMT/PP for convenience, where x represents the weight content of clay in PE-MMT phase. Furthermore, HSIM was also employed to prepare neat PE, blends of PP with PE at weight proportion of 5:5 (marked as PE/PP) and PE-MMT nanocomposites with different clay contents (marked as PE-xMMT), respectively, as reference.

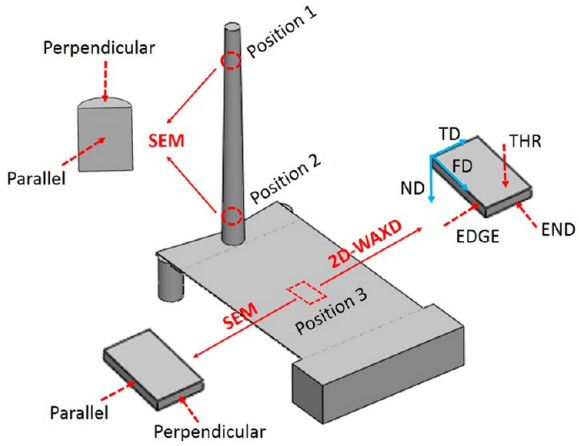

Figure 1. Schematic of injection molded sample. The positions used for characterization are indicated.

2.3. Characterization. *2.3.1. Scanning Electron Microscope (SEM).* SEM was used to observe the morphology of polymer nanocomposites and the dispersion status of clay. These samples were cryogenically fractured after immersing in liquid nitrogen for 2h. After that, they were chemically etched with 3% solution of potassium permanganate in a 2:1 (by volume) mixture of concentrated sulfuric acid and 85% orthophosphoric acid. PP phase was selectively etched due to its weaker resistance to the mixed acid.[29] After that, these specimens were washed, dried and gold-coated to study the phase

DOI: 10.1021/acsami.5b00347
ACS Appl. Mater. Interfaces 2015, 7, 10178−10189

morphology as well as clay dispersion using SEM (FEI Inspect F) with an accelerating voltage of 20 kV.

2.3.2. Rheological Measurements. The rheological measurements were carried out on a piston-mode Rosand RH70 (Malvern, Bohlin Instruments) capillary rheometer under 200 °C. The selected shear rate for measurement is in the range of 100−3800 s^{-1}.

2.3.3. Differential Scanning Calorimetry (DSC). Thermal analysis of these samples was conducted using a Perkin−Elmer DSC pyris-1, indium calibrated. Melting endotherms were obtained at 10 °C/min with 4−6 mg of sample in nitrogen atmosphere. For the purpose of comparison with neat polymer, the crystallinity X_c of component i in the blends can be normalized using the equation

$$X_c = \frac{\Delta H_i}{\Delta H_i^m \phi_i} \tag{1}$$

where ΔH_i is the enthalpy of fusion of component i, directly obtained from DSC, and ϕ_i is the mass fraction of component i in the blends. The enthalpy of fusion ΔH_i^m of 100% crystalline polymer is 293 and 207 J/g for HDPE and iPP, respectively.[29]

2.3.4. Transmission Electron Microscopy (TEM). Clay dispersion in nanocomposite samples was characterized using TEM (FEI-TecnaiG2 F20 S-TWIN type transmission microscope) operated at 200 kV. Ultrathin slices of 80 nm thickness were obtained by cryo-microtoming along the flow direction of these samples using a Leica microtome at −80 °C.

2.3.5. Two-Dimensional Wide-Angle X-ray Diffraction (2D-WAXD). 2D-WAXD measurements were conducted on a Bruker DISCOVER D8 diffractometer. To obtain 3D-analysis of such oriented microstructure, the X-ray beam was irradiated on the specimen from three directions: THR, EDGE, and END, as shown in Figure 1. Strips with 400 μm thickness were microtomed using Leica microtome before measurement was conducted. XRD data were collected for each point on the sample at ambient temperature using Cu Kα radiation for 180 s. The background of all 2D-WAXD patterns used in this article had been extracted and thus allow a qualitative comparison between various specimens. To give a more accurate description on the orientation degree of clay platelets, azimuthal scan of (001) lattice plane of clay platelets was performed with a step of 1° from 0 to 360° and the full width at half-maximum (fwhm) were calculated.

2.3.6. Oxygen Gas Permeability Measurement. The oxygen gas permeability test was performed using a VAC-V1 gas permeability tester (Labthink Instrument Co., China) at 40 °C and 50% relative humidity (RH) according to ISO15105-1:2007, based on the pressure difference method. During measurement, a circular sheet with a diameter of 50 mm was mounted in the gas permeation cell to form a sealed barrier between two chambers, that is, lower chamber with high vacuum pressure and upper chamber containing high-purity oxygen at atmospheric pressure. The permeability coefficient (P) of oxygen that permeated through the sheet (5 cm^2 in measuring area) from upper chamber to lower one was determined by monitoring the pressure variations with time in the lower chamber. To ensure the reproducibility of these results, three independent specimens were tested for each sample.

2.3.7. X-ray Diffraction (XRD). XRD analysis was performed with a PhilipsX'Pert PRO diffractometer (Holland) with Cu Kα radiation(λ = 0.154 nm) at room temperature.

2.3.8. Contact Angle Measurements. Contact angle measurements were carried out in a sessile drop mold with KRUSS DSA100. The sample for contact angle measurement was compression molded at 200 °C under a pressure of 8 MPa for 6 min then cooled to 20 °C. Moreover, the MMT film for contact angle experiment was prepared by the following procedure: 1 g of MMT was added into 50 mL ethanol, the mixture was then subjected to sonication for 5 min. After that, 6 mL of supernatant was suffered to suction filtration and thus obtain the MMT thin film on the surface of filter membrane. Contact angles were measured on 3 mL of wetting solvent at 20 °C, and the results reported were mean values of 3 replicates. The surface tensions, dispersion and polar components of these specimens can be obtained from these measurements. Furthermore, the interfacial tension between PP and PE or PE-MMT composites could be calculated from the surface tensions of different components using the harmonic-mean equation

$$\gamma_{12} = \gamma_1 + \gamma_2 - 4\left(\frac{\gamma_1^d \gamma_2^d}{\gamma_1^d + \gamma_2^d} + \frac{\gamma_1^p \gamma_2^p}{\gamma_1^p + \gamma_2^p}\right) \tag{2}$$

where γ_1, γ_2 are the surface tensions of components 1, 2; γ_1^d, γ_2^d are the dispersive parts of the surface tensions of components 1, 2; and γ_1^p, γ_2^p are the polar parts of the surface tensions of components 1, 2.

3. RESULTS AND DISCUSSION

3.1. Formation of Alternating Multilayer Structure. Shear flow has been reported to have profound influence on the phase behavior, such as phase morphology, phase mixing or demixing, and phase inversion of polymer blends.[30−33] For immiscible blends, shear-induced microstructural changes include phase deformation, coalescence, retraction, and different types of breakup. It is controlled by hydrodynamics, rheology of polymer components and droplet−droplet interactions.[32] Therefore, it is necessary to characterize the interfacial tension and viscosity change after the incorporation of nanoclay into PE phase.

3.1.1. Rheology. Capillary rheometer has been empolyed to investigate the rheological behavior of these polymer components and blends. As shown in Figure 2, the viscosity

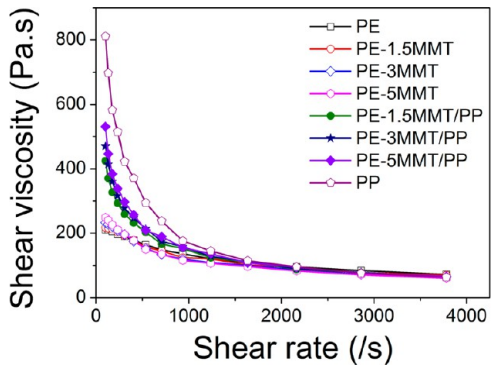

Figure 2. Shear viscosity of neat PE, PP, and a series of binary and ternary composites as a function of shear rate.

increases with clay content at low shear rate region. A typical shear thinning behavior can be observed for all samples at high shear rates. As the shear rate exceeds 2 × 10^3 s^{-1}, all samples show comparable viscosity and it decreases slowly with increasing shear rate. As calculated in our previous paper,[34] such high shear rate is easily achivable in HSIM process. Therefore, it is rational to conclude that good viscosity match could be still preserved upon addition of nanoclay into these systems during HSIM process. It should be noted that the shear viscosity of ternary blends at lower shear rate is between that of neat PP and binary blends. This is thought as a rule of mixture effect between different polymer melt.[35] Moreover, the initial shear viscosity of PE-MMT composits and neat PE are almost similar. MMT based polymer composites have been studied extensively in the literature. It is often observed that the viscosity of PE-MMT is only slightly increased comparing with neat PE.[36,37] Therefore, the difference between neat polymer and PE-MMT is even smaller at shear rate of 100 s^{-1} (which is the initial shear rate in Figure 2) because of shear thinning effect. For ternary blends, it is noted that the initial shear

DOI: 10.1021/acsami.5b00347
ACS Appl. Mater. Interfaces 2015, 7, 10178−10189

Table 1. Contact Angle, Surface Tension, and Interfacial Tension Results of Neat PP, PE, and PE-3MMT

	contact angle (deg)		surface tension (mN/m)			
sample	water	diiodomethane	total (γ)	dispersion component (γ^d)	polar component (γ^p)	interfacial tension with iPP (mN/m)
PP	57.2	43.8	54.70	34.76	19.94	
PE	45.48	58.57	55.85	37.64	18.20	0.20394
PE-3MMT	29.13	35.86	56.12	38.52	17.60	0.33879

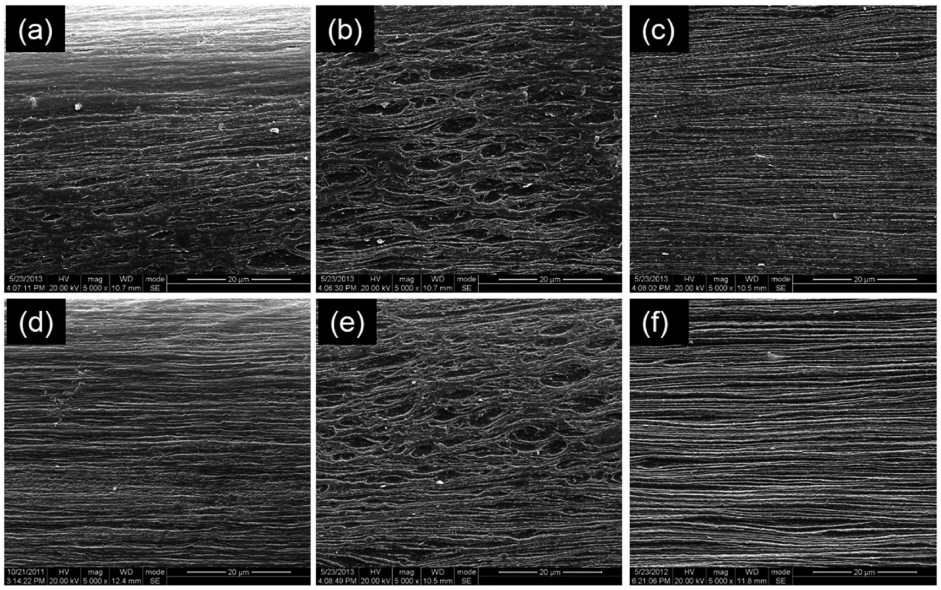

Figure 3. SEM micrographs of PE-3MMT/PP viewed parallel (top column) and perpendicular (bottom column) to flow direction: (a, d) skin layer, (b, e) intermediate layer, and (c, f) core layer.

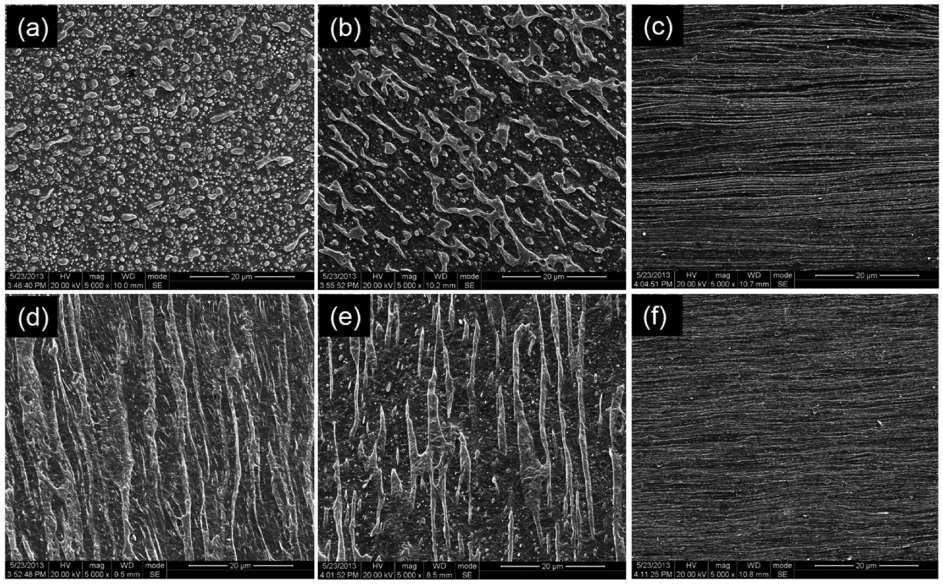

Figure 4. SEM micrographs of PE-3MMT/PP viewed parallel (top column) and perpendicular (bottom column) to flow direction: (a, d) position 1, (b, e) position 2, and (c, f) position 3.

viscosity is higher for higher MMT content. But the effect of MMT on shear viscosity is disappeared at higher shear rate.

3.1.2. Interfacial Tension. As shown in Table 1, the interfacial tension between PP and PE has been characterized through contact angle measurement. It is demonstrated that the incorporation of clay into PE phase has little influence on the interfacial tension. Therefore, it is reasonable to conclude that the dispersed phase will still be subjected to intense deformation and difficult to recover its initial morphology with such low interfaical tension.[38]

3.1.3. SEM. SEM studies were carried out to investigate the hierarchical structure of PE-3MMT/PP injection molded part. The complete cross section of the sample viewed parallel to flow direction is shown in Supporting Information Figure S1. Three layers could be distinguished as skin layer, intermediate layer and core layer, which accounts for around 50%, 20% and

DOI: 10.1021/acsami.5b00347
ACS Appl. Mater. Interfaces 2015, 7, 10178−10189

30% regarding the whole sample thickness, respectively. It is noteworthy that such high ratio for skin layer should be attributed to the intense shear field and extremely high cooling rate during filling phase.[39] The detailed morphology of various layers is shown in Figure 3. The skin layer presents irregular layer structure with nonuniform thickness of each layer, which might be caused by a balance between intense shear field and fast cooling rate. Typical cocontinuous structure with slight orientation parallel to the sample surface is observed in intermediate layer. In the core layer, a delicate multilayered structure with alternating PE-MMT and PP phase elongated parallel and perpendicular to the flow direction could be observed. This is similar to the morphology obtained in our previous studies.[28,34] The alternating multilayered structure has regular arrangement, uniform thickness for each single layer, and high length to thickness ratio. It is demonstrated that the addition of clay could barely influence the formation of multilayer structure. Furthermore, few agglomerates could be observed, which implies that the clay was well dispersed in the nanocomposites. It should be noted that the thickness of these layers are between 70 and 400 nm according to SEM measurement shown in Figure S3 (see in Supporting Information).

The phase structure evolution at different location and injection runner have also been systematically examined to further investigate the formation mechanism of alternating multilayered structure as shown in Figure 4 for positions 1−3 illustrated in Figure 1. At position 1, PE-MMT shows fiber-like morphology as dispersed phase. These fibers were merged into each other and form coarse discontinuous layer sturcture at position 2. At position 3, these discontinuous layers further converged and well arranged parallel to the flow direction, thus formed more continuous and dense layered structure with large length to thickness ratio. The high injection speed as well as large ratio between runner cross section and thin mold cross section (around 20) is believed to trigger extremely high shear rate to multicomponent polymer mixtures and thus induce the formation of alternating multilayered structrue. Furthermore, fast cooling rate in such thin mold wall also plays a crucial role since the short relaxation time is not adequate for the deformed polymer phase to restore its original morphology.

3.2. Dispersion and Distribution of Clay in the Nanocomposites. The dispersion of these MMT layers in the nanocomposites is of great importance for optimizing mechanical, thermal and gas barrier property. Intercalated and exfoliated layered silicate nanocomposites, as two extreme states of nanoplatelets dispersion, are often used to describe the dispersion morphology of silicate layers. Intercalation implies the insertion of polymer chains in the galleries of initial layered tactoids, which leads to longitudinal expansion of galleries as well as increase in interlayer spacing. Exfoliation implies complete breakage of the initial layer stacking order and homogeneous dispersion of these layers in the polymer matrix. The latter case presents much higher values for tortuosity factor and aspect ratio of impermeable nanoplatelets, which leads to enhanced diffusion pathway.[25] However, it is difficult to obtain well exfoliated nanocomposite structure in nonpolar polymers such as polyolefins. A number of efforts have been devoted to enhance the interfacial interactions between clay and polyolefin matrix by adding modified polymers with polar groups (compatibilizers) and thus improve clay dispersion.[40−42]

For current system, a widely used compatibilizer: maleic anhydride grafted PE, was used to promote the dispersion of silicate layers. X-ray diffraction curves shown in Figure 5 are utilized to demonstrate the dispersion status of clay. Two

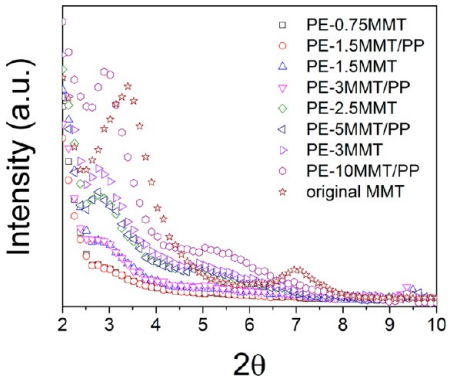

Figure 5. XRD curves of the pristine clay and as-prepared nanocomposites.

diffraction peaks could be observed for pristine organic clay corresponding to the basal spacing d_{001} = 2.52 nm (2θ = 3.5°) and d_{002} = 1.26 nm (2θ = 7°), respectively. In PE-0.75MMT, PE-1.5MMT/PP, PE-1.5MMT, PE-3MMT/PP, PE-2.5MMT, PE-5MMT/PP, and PE-3MMT the diffraction peak of (001) lattice plane are almost the same, with lower angles (2θ = 2.8°) with different intensity due to different filler content. This implies that the polymer chains have been well inserted in the interlayer of tactoids with the aid of compatibilizer and give rise to the expansion of galleries with interlayer spacing of d_{001} = 3.15 nm. Furthermore, the diffraction peak of (002) lattice plane is almost disappeared. It should also be noted that the diffraction curves for PE-0.75MMT, PE-1.5MMT, and PE-2.5MMT are almost overlapping with PE-1.5MMT/PP, PE-3MMT/PP, and PE-5MMT/PP, respectively, due to the same overall filler content as well as similar status for filler dispersion. For PE-10MMT/PP, it is clearly observed that the lower angle at (2θ = 2.93°), indicating reduced interlayer spacing (3.01 nm) caused by aggregation of MMT at higher filler content. TEM was also employed to further evaluate the structure of clay nanoplatelets in PE-3MMT/PP and PE-1.5MMT as displayed in Figure 6. Partial exfoliated/partial intercalated clay structure is observed for both nanocomposites. The intercalated tactoids are a few tens of nanometers thick and several hundred nanometers long while the exfoliated single platelets exhibit a thickness of several nanometers and a length of 100 nm. Moreover, well alignment along injection direction could be

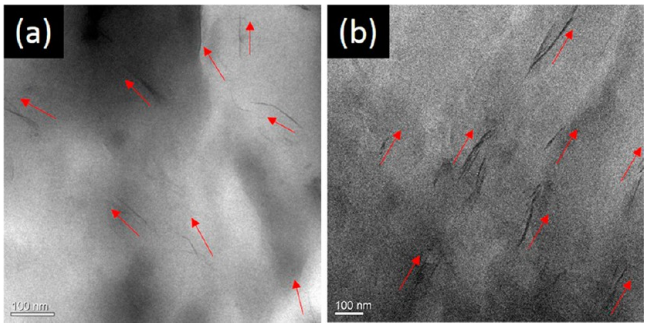

Figure 6. TEM images of as-prepared PE-1.5MMT (a) and PE-3MMT/PP (b) nanocomposites. Red arrows indicate the orientation of clay nanoplatelets.

DOI: 10.1021/acsami.5b00347
ACS Appl. Mater. Interfaces 2015, 7, 10178−10189

observed in PE-3MMT/PP, which might be caused by the strong shear field induced orientation as well as the possible orientation confinement subjected to these nanoplatelets by layered structure. Meanwhile, the nanoplatelet exhibits much less orientation in PE-1.5MMT. Such issue will be further discussed in the next section.

As well-known, the selective localization of nanofiller in polymer blends is commonly explained by the concept of wetting coefficient.[43] In equilibrium state, the localization of MMT in polymer blends can be predicted by the minimization of interfacial energy. According to Young's equation, it is possible to find the equilibrium position of MMT by evaluating the wetting coefficient ω_a, the wetting coefficient is most commonly interpreted in a way that, for value < −1, the fillers are predicted to be located in the polymer phase named first (here PE), and for value > 1, in the polymer phase named second (here PP). In the interval of ω_a value between −1 and 1, the fillers are predicted to be located at the interface. The detail for such calculation can be found in our previous paper.[44]

From contact angle measurements, the total surface tension of MMT is 23.63 mN/m, which is comparable to the results reported in literature.[45] The calculated wetting coefficients are below −1 (see in Table 2), as the interfacial energy between PE and MMT (γ_{PE-MMT}) is slightly lower than that between PP and MMT (γ_{PP-MMT}), which indicates a slightly better wetting of MMT with PE. Therefore, the PE−MMT pair tends to be formed to minimize the total free energy in the ternary composite of PE-MMT/PP. It should be noted that the effect of PE-*g*-MA is not considered in this calculation. Such issue will further help clay stay in the PE phase.

Table 2. Interfacial Energies and Wetting Coefficients As Calculated Using Harmonic Mean Equations

	interfacial energies (mN/m)			
calculation methods	γ_{PE-MMT}	γ_{PP-MMT}	γ_{PE-PP}	wetting coefficient (ω_a mN/m)
harmonic mean equation	28.83	29.55	0.20	−3.6

To further study the possible confinement of clay in the layered structure, it is important to confirm if these clays had migrated from PE phase to PP phase under intense and complex flow field during processing. Clay nanoplatelets have been recognized to greatly influence the crystallization behavior of polymer matrix.[46−49] Therefore, DSC study was used as an indirect method to characterize the distribution of these silicate layers. Figure 7 shows the melting curves and crystallinity analysis of the prepared PE/PP and PE-MMT/PP with different filler content. It is observed that the melting endotherms of all samples illustrate two melting peaks. The peak located at 130 °C is contributed by the melting of PE crystals, while the other peak at 165 °C is ascribed to the melting of α PP crystal. The location of PE melting peak as well as PP α crystals were barely influenced by clay. However, an obvious intensity decrease in the PE crystals could be observed upon clay loading. A further quantitative estimation demonstrated that the crystallinity of PE decreased from 57.4% for neat PE/PP to 56.5%, 45.0%, 47.7%, and 40.3% for PE-MMT/PP containing 1.5, 3, 5, and 10 wt % in the PE phase of these ternary blends, while the crystallinity of PP has been barely affected as shown in Figure 7b. Hence, it is concluded that clay nanoplatelets are selectively distributed in PE phase. Several possible mechanisms might be responsible for this: the predispersion of clay in PE, the moderate intense mixing effect in single screw extruder and the compatibilizer tethered to clay nanosheets is maleic anhydride grafted PE which has better affinity with PE. The mechanism for the decrease in PE crystallinity has been reported in literature:[46] the interactions between clay and PE matrix would act to reduce the mobility of crystallizable chain segments and thus leads to an impressive crystallinity decrease. To further confirm the location of MMT, extra SEM study has been performed. As shown in Supporting Information Figure S3, MMT are clearly observed in unetched PE phase. This agrees well with DSC study and discussion. Similarly, the preference of PE phase in PP/PE blends has also been reported for different fillers including: CB[50] and CNTs.[51] It is proposed that filler was selectively located in a polymer with a lower T_g arising from that for polymers having a similar carbon−carbon main chain, a lower T_g was generally related to a higher flexibility of chains and thus a low entropic loss for adsorption on the CB surface.[50] It should be pointed that PP/PE specimens could not be stained to distinguish between PP and PE phase in TEM due to the similarity in their polymer chains. In TEM images shown in Figure 6b, it is demonstrated that the space between oriented MMT layers are correlated with the layer thickness observed in Supporting Information Figure S3. Therefore, the selective localization of MMT in PE phase is confirmed.

3.3. Orientation Behavior of Clay Nanoplatelets. The orientation behavior of nanoclay in PE-1.5MMT and PE-

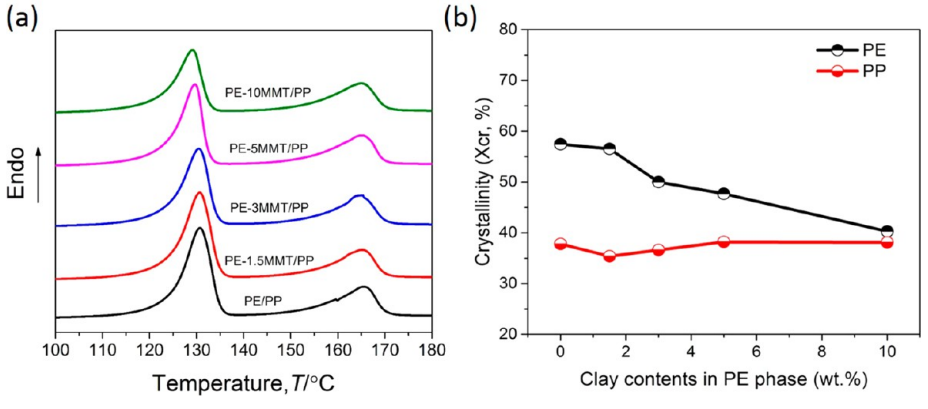

Figure 7. DSC heating curves (a) and crystallinity analysis (b) of the prepared samples.

DOI: 10.1021/acsami.5b00347
ACS Appl. Mater. Interfaces 2015, 7, 10178−10189

3MMT/PP nanocomposites are investigated with 2D-WAXD as shown in Figure 8. THR, END, and EDGE views are

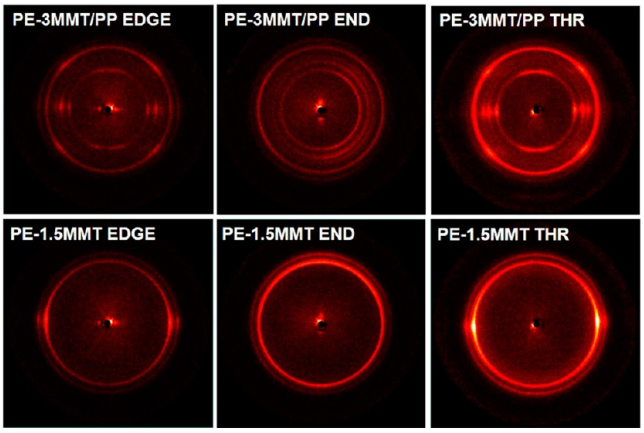

Figure 8. 2D-WAXD patterns of PE-3MMT/PP (top column) and PE-1.5MMT (bottom column) nanocomposites detected in 3D spacings.

illustrated in Figure 1. It could be observed that, for both PE-1.5MMT and PE-3MMT/PP, a pair of intensive streaks near the stopper, representing the *d*-spacing of clay stacks, emerged on the equator of EDGE view and the meridian of END view. On the other hand, the reflection corresponding to the ordered stacking of clay is quite feint in the THR view image for both nanocomposites. These scattering characteristics indicates that an in-plane orientation of clay nanoplatelets with the their surface parallel to the molded part surface.[52,53] To give a further quantitative evaluation on the orientation level of these nanoplatelets, the azimuthal scans of (001) lattice plane of clay have been plotted in Figure 9 and the fwhm have been

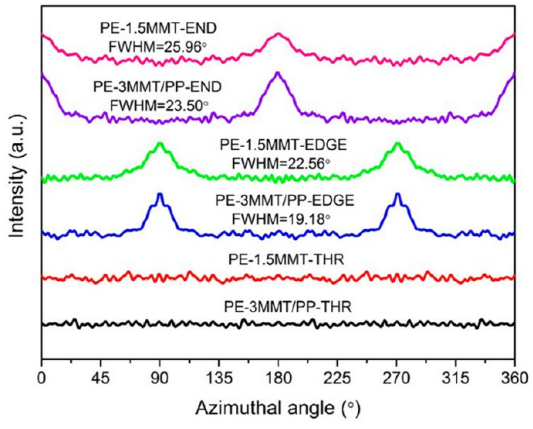

Figure 9. Azimuthal scan of (001) plane of OMMT in the PE-1.5MMT and PE-3MMT/PP nanocomposites detected in the EDGE view and END view.

calculated from the azimuthal scan curves in the EDGE and END view. For PE-3MMT/PP and PE-1.5MMT, the fwhm of peaks located at 90° azimuth (equator) in the EGDE view are 19.18° and 22.56°, respectively. As to the END view, the fwhm of peaks located at 0° azimuth (meridian) are 23.50° and 25.96°, respectively. Meanwhile, the intensity of *d*-spacing reflection of clay tactoids are quite weak for both nanocomposites in the THR view. It is noted that the orientation degree of clay in PE-1.5MMT are lower than that in PE-3MMT/PP for both EDGE and END views. This indicates that PE-1.5MMT exhibits lower orientation level of clay nanoparticles parallel to the flow direction revealed in the EDGE view and less ordering degree of tactoids assembling displayed in the END view compared with PE-3MMT/PP. Comparing with the uniplanar-axial orientation of clay tactoids with the tactoid surface parallel to molded part surface (FD-TD plane) in PE-3MMT/PP, the tactoids in PE-1.5MMT tend to rotate their surface to a certain extent inside the nanocomposites. This is in accordance with the above-mentioned TEM observation.

The orientation behavior of layered silicate during processing is usually influenced by shear field, temperature gradient and phase microstructure.[11,54] In the case of HSIM, the intense shear flow could easily induce the orientation of nanoparticles. Furthermore, the insufficient time for the relaxation of nanoplatelets due to high cooling rate is also beneficial for preserving the orientation. Assuming the same shear gradient and temperature field during HSIM process for PE-1.5MMT and PE-3MMT/PP nanocomposites, it is reasonable to speculate that the phase morphology might be exclusively responsible for the different orientation level observed. The alternating multilayer structure obtained in PE-3MMT/PP might play a critical role in contributing higher orientation level. The tumbling and rotation of these nanoplatelets were certainly restricted in these PE-MMT layers with a layer thickness in the range of 70−400 nm. Furthermore, the layer structure of PE-MMT phase also enforces these nanoparticles to orient parallel to the part surface during the formation of alternating multilayer structure. As for PE-1.5MMT, these nanoparticles have adequate space to turn their surfaces without the confinement of layered structure. Therefore, it is rational to propose that the higher orientation degree of clay platelets obtained in PE-3MMT/PP might arise from the confinement effect of alternating multilayer structure.

3.4. Oxygen Barrier Properties. To investigate the barrier properties of these materials, oxygen permeability are characterized as shown in Figure 10 and Table 3. It is demonstrated that the permeability of PE/PP with alternating multilayer structure shows little change comparing with neat PE specimen. This might be interpreted that the thickness of each layer is not enough to significantly change crystal superstructrue as well as the lamellae arrangement to remarkably increase the gas diffusion pathway. As shown in Figure 10, systematic comparisons have been made between different specimens containing different MMT content. In Figure 10 a, PE-1.5MMT/PP, PE-3MMT/PP, PE-5MMT/PP, and PE-10MMT/PP are compared with neat PE and PE/PP, it is demonstrated that the barrier property is enhanced with increasing filler content until PE-5MMT/PP. There is some decrease in barrier property while MMT content in PE is increased from 5 to 10 wt % because of possible aggregation of MMT at high filler content. Such phenomenon is often observed for nanocomposites with relative higher filler content.[55−57] In Figure 10 b, ternary blends are compared with binary composites containing the same overall filler content. It is demonstrated that all ternary blends have better barrier property due to better orientation and confined morphology. In addition, remarkable permeability decrease by 45.7% is observed in PE-3MMT/PP, which is obviously superior to that of PE-1.5MMT with the same overall 1.5 wt % clay content. Comparing to other PE based nanocomposites filled with clay (as listed in Table 3), PE-3MMT/PP demonstrates the most notable oxygen barrier property

DOI: 10.1021/acsami.5b00347
ACS Appl. Mater. Interfaces 2015, 7, 10178−10189

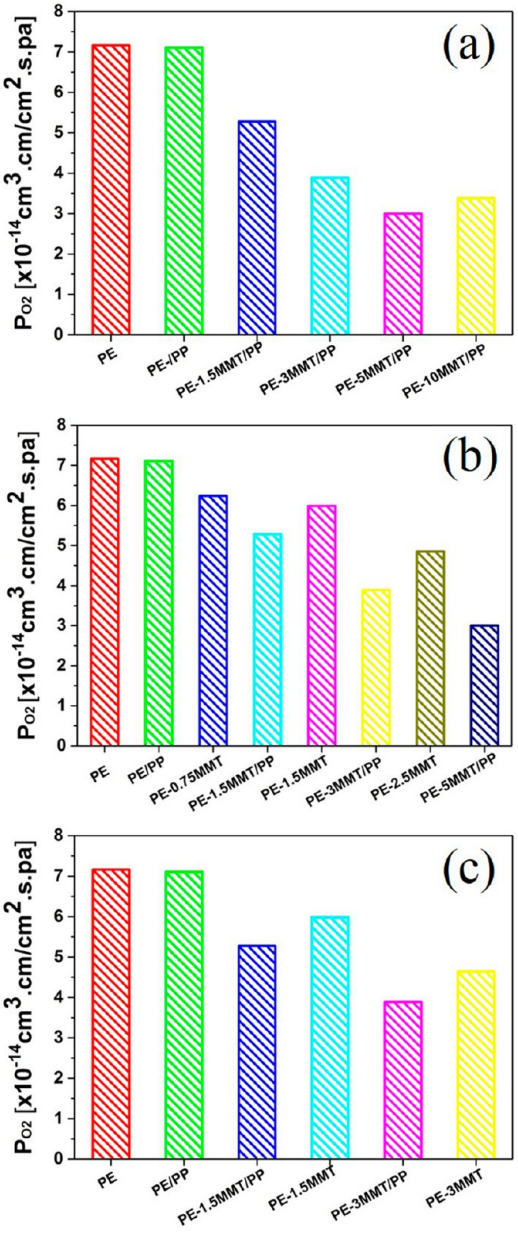

Figure 10. (a) Permeability coefficient of neat PE, PE/PP and ternary composites as a function of MMT content. (b) Comparison of the permeability coefficient between ternary blends and binary composites containing the same overall filler content. (c) Comparison of the permeability coefficient between ternary blends and binary composites containing twice the filler content in the latter.

enhancement by 45.7% with comparable clay content of 1.5 wt %. Such improvement is even comparable to the highest permeability decrease with high clay content in other PE based nanocomposites. Furthermore, PE-5MMT/PP with an overall 2.5 wt % clay content in the nanocomposites could enhance the permeability by 58.2%. This is the largest enhancement in the barrier property for polyolefin based composites to be best of our knowledge. It should be noted that the permeability of neat polymer used in this study is almost 1 order of magnitude lower than the values reported in literature. This might be caused by the intense orientation of macromolecule chain as demonstrated in 2D-WAXD results (Figure 8).[58−61] Then, the actually permeability of these nanocomposites in current study is even lower than the results in literature. This indicates such a method is very effective at fabricating high performance barrier materials. As shown in Figure 10 c, PE-1.5MMT/PP and PE-3MMT/PP are compared with PE-1.5MMT and PE-3MMT, respectively. It is demonstrated that even with twice the filler content in these binary composites, better barrier property is obtained for ternary composites. This has confirmed the effect of filler orientation is much more important than filler content in this system.

The barrier property of semicrystalline polymer-based nanocomposites are not only controlled by the impermeable nanoplatelets but also depends on the crystallinity of polymer matrix. The crystalline region could be considered as impermeable phase dispersed in the permeable amorphous phase. The improvement on gas barrier property of semicrystalline polymer through increasing crystallinity could be interpreted as follows: the gas solubility could be reduced by the formation of lamellar crystals due to the insolubility of gas in the crystalline phase. Meanwhile, the gas molecules have to follow more tortuous paths around the impermeable lamellas.[66−68] In current study, as listed in Table 4, a significant decrease in PE crystallinity and unchanged PP crystallinity is obtained in PE-MMT/PP nanocomposites comparing with PE/PP, which should contribute to poorer barrier property. Therefore, it is concluded that the improved barrier property in current system is mainly caused by the impermeable nanoplatelets rather than the crystallinity of polymer. It is interesting to note that the crystallinity of PE in PE-1.5MMT/PP varies slightly comparing to neat PE. This is obviously different from the case that crystallinity decreases a wider margin upon 3 wt % or more clay loading into the PE phase of PE/PP. This might be ascribed by the formation of clay network with 3 wt % content in PE phase as the viscoelastic properties revealed in Supporting Information Figure S2. It is observed that clay addition increases the storage modulus (G') and this effect is especially more pronounced at low frequencies. However, the enhancement of G' for PE-1.5MMT is faint at low frequency region while a large magnitude of G' increase and slope of G' decrease could be observed for PE-3MMT, which is probably due to the increase in interfacial area between nanoclays and PE matrix or enhancement in the physical interactions between nanoclay platelets.[69,70] The G' of PE-7MMT and PE-10MMT becomes frequency independent at low frequencies, which is the characteristic behavior of solid-like materials due to the physical network formation. Therefore, the strong interactions between PE and nanoclay in PE-3MMT/PP could be responsible for the mobility reduction in crystallizable chain segments and thus result in crystallinity decrease in a large amplitude.

3.4.1. Mechanism. Therefore, considering the comparable clay dispersion status (as indicated in Figures 5 and 6), as well as the same overall clay content, the higher orientation degree of these nanoplatelets is thought to be the mechanism for lower permeability of these ternary PE-MMT/PP composites in comparison with binary PE-MMT. Comparing with the nonuniform orientation of these nanoparticles in PE-1.5MMT, these impermeable nanoplatelets are more regularly arranged in a parallel array with their main direction perpendicular to the diffusion direction in PE-3MMT/PP, which could maximize the tortuostity. The alternating multilayer structure is believed to be responsible for such strong in-plane orientation of these nanoplatelets. As the layered structure could impose confinement on the nanoplatelets restricting their rotation and tumbling. Moreover, PE-3MMT/

DOI: 10.1021/acsami.5b00347
ACS Appl. Mater. Interfaces 2015, 7, 10178−10189

Table 3. Comparison of the Oxygen Barrier Properites for PE-Based Nanocomposites Filled with Clay

polymer matrix	P_{O_2} of polymer matrix without clay ($cm^3 \cdot cm/cm^2 \cdot s \cdot pa$)	comparable clay *fc* (wt %)	P_{O_2} enhancement at comparable clay *fc* (%)	clay *fc* at highest P_{O_2} enhancement (wt %)	highest P_{O_2} enhancement (%)
LDPE/LLDPE (70/30)[62]		1.8	27.40	3.54	38.70
LLDPE[40]	4.02×10^{-13}			4.76	55
LLDPE[63]	2.55×10^{-13}	2	14.70	4	44.10
metallocene PE[64]				5	41.10
LDPE-*g*-MA[64]	/			19.3	38.28
LLDPE[37]	4.16×10^{-13}	0.8 and 2.5	14.4 and 19.6	6.9	42
LDPE[41]	3.80×10^{-13}	1	2.63	7	24
HDPE[65]	7.55×10^{-13}	1.96	4.17	3.85	7.11
HDPE-*g*-Si[65]	7.68×10^{-13}	1.96	32.50	3.85	40.70
cross-linked HDPE[65]	6.36×10^{-13}	1.96	26.50	3.85	36.00
this study	$\mathbf{7.16 \times 10^{-14}}$	**1.5**	**45.70**	**2.5**	**58.2**

Table 4. Crystallinity of the Prepared Samples Derived from DSC Heating Curves

sample	PE	PE/PP	PE-1.5MMT/PP	PE-3MMT/PP	PE-5MMT/PP	PE-10MMT/PP
PE Xcr	55.8	57.4	56.5	45.0	47.7	40.3
PP Xcr		37.8	35.4	36.6	38.2	38.1

PP exhibits obviously higher local density of clay platelets due to double relative clay content in PE phase as well as the phase morphology induced denser packing structure of these nanoplatelets. These nanoplatelets form a tightly packed brick-like wall structure, which is also beneficial for decreasing possible oxygen pathway. Therefore, the superior barrier property of ternary PE-MMT/PP in comparison with binary PE-MMT nanocomposites should be understood as the combination of better in-plane orientation level and denser assembling morphology of nanoplatelets. The schematic representation shown in Figure 11 illustrates the oxygen barrier mechanism for ternary PE-MMT/PP and binary PE-MMT nanocomposites to give a more vivid description. Importantly, by comparing ternary and binary composites with the same relative MMT content in PE phase, it is demonstrated that the orientation of MMT play much more imporant role in barrier property than higher overall MMT content.

4. CONCLUSION

In conclusion, we present a simple and efficient strategy to enhance the barrier property by confining impermeable MMT into alternating multilayered structure through HSIM. It is thought that the formation of alternating multilayered structure is caused by the low interfacial tension and good viscosity match between PE-MMT and PP in such polymer blends. Through a number of characterizations, MMT are demonstrated to be selectively dispersed in PE phase and illustrate partial exfoliated/partial intercalated dispersion status. 2D-WAXD analysis indicates that ternary PE-MMT/PP composite exhibits an uniplanar-axial orientation of clay tactoids with their surface parallel to mold surface while the tactoids in binary PE-MMT composite with the same overall clay contents tend to rotate their surface to a certain extent. The better orientation level of nanoclay in PE-MMT/PP could be attributed to the confinement of alternating multilayer structure, which restricts the tumbling and rotation of nanoplatelets. Therefore, the oxygen barrier property of PE-MMT/PP is superior to that of PE-MMT (even if only half of the overall MMT content is contained in ternary composites) due to increased turtosity of gas permeation pathway for the former containing more regular clay array with their main direction perpendicular to the diffusion direction. This has clearly illustrated that confinement and orientation is more important than higher filler content. Moreover, the alternating multilayered structure and local higher density of nanoplatelets could induce denser assembling morphology of nanoclay and thus construct a tightly packed brick-like wall structure, which is also responsible for the improvement in barrier property. Comparing with the results in literature for PE based composites, the improvement in barrier property achieved (45.7% and 58.2% improvement with 1.5 and 2.5 wt % MMT content, respectively) here is outstanding. This study has shed some light on efficient and easy fabrication of

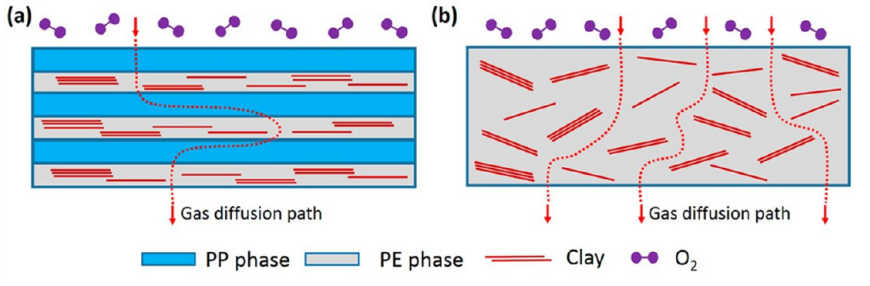

Figure 11. Schematic representation showing the possible oxygen barrier mechanism for PE-3MMT/PP (a) and PE-1.5MMT (b) nanocomposites.

DOI: 10.1021/acsami.5b00347
ACS Appl. Mater. Interfaces 2015, 7, 10178−10189

polymer sheets with excellent barrier performance and other functional materials require layered structure.

■ ASSOCIATED CONTENT

Supporting Information

Additional three figures showing the SEM micrographs of the complete cross section of PE-3MMT/PP, viscoelastic properties of PE-MMT composites with different clay contents, and SEM images showing the thickness for different ternary composites. The Supporting Information is available free of charge on the ACS Publications website at DOI: 10.1021/acsami.5b00347.

■ AUTHOR INFORMATION

Corresponding Authors

*E-mail: huadeng@scu.edu.cn. Tel: +86-28-85460953.
*E-mail: qiangfu@scu.edu.cn. Tel. +86-28-85401795.

Author Contributions

F.Y. and H. D. contributed equally to this work and should be considered cofirst authors.

Notes

The authors declare no competing financial interest.

■ ACKNOWLEDGMENTS

We express our sincere thanks to the National Natural Science Foundation of China for financial support (51273117 and 51421061). H.D. would like to thank the Ministry of Education (Program for New Century Excellent Talents in University, NCET-13-0383), the Innovation Team Program of Science & Technology Department of Sichuan Province (2014TD0002), and Sichuan Province for financial support (2013JQ0008). We would like to thank Mr. Yi Zhou for carrying out sample preparation and characterization presented in Figures 5, 7, and 10.

■ REFERENCES

(1) Sadovoy, A. V.; Lomova, M. V.; Antipina, M. N.; Braun, N. A.; Sukhorukov, G. B.; Kiryukhin, M. V. Layer-by-Layer Assembled Multilayer Shells for Encapsulation and Release of Fragrance. *ACS Appl. Mater. Interfaces* **2013**, *5*, 8948−8954.

(2) Danlee, Y.; Bailly, C.; Huynen, I. Thin and Flexible Multilayer Polymer Composite Structures for Effective Control of Microwave Electromagnetic Absorption. *Compos. Sci. Technol.* **2014**, *100*, 182−188.

(3) Su, L.; Chen, Y.; Chen, M. Dual Drug-Eluting Stents Coated with Multilayers of Hydrophobic Heparin and Sirolimus. *ACS Appl. Mater. Interfaces* **2013**, *5*, 12944−12953.

(4) Yang, Y.; Haile, M.; Park, Y. T.; Malek, F. A.; Grunlan, J. C. Super Gas Barrier of All-Polymer Multilayer Thin Films. *Macromolecules* **2011**, *44*, 1450−1459.

(5) Xiang, F.; Tzeng, P.; Sawyer, J. S.; Regev, O.; Grunlan, J. C. Improving the Gas Barrier Property of Clay−Polymer Multilayer Thin Films Using Shorter Deposition Times. *ACS Appl. Mater. Interfaces* **2013**, *6*, 6040−6048.

(6) Jordan, A. M.; Lenart, W. R.; Carr, J. M.; Baer, E.; Korley, L. T. J. Structural Evolution during Mechanical Deformation in High-Barrier PVDF-TFE/PET Multilayer Films Using in Situ X-ray Techniques. *ACS Appl. Mater. Interfaces* **2014**, *6*, 3987−3994.

(7) Lee, P. C.; Dooley, J.; Robacki, J.; Jenkins, S.; Wrisley, R. Improvements in Flex Oxygen Barrier Properties of Polymeric Films by Microlayer Coextrusion. *J. Plast. Film Sheeting* **2014**, *30*, 234−247.

(8) Wang, H.; Keum, J. K.; Hiltner, A.; Baer, E.; Freeman, B.; Rozanski, A.; Galeski, A. Confined Crystallization of Polyethylene Oxide in Nanolayer Assemblies. *Science* **2009**, *323*, 757−760.

(9) Gupta, M.; Lin, Y.; Deans, T.; Baer, E.; Hiltner, A.; Schiraldi, D. A. Structure and Gas Barrier Properties of Poly(Propylene-Graft-Maleic Anhydride)/Phosphate Glass Composites Prepared by Microlayer Coextrusion. *Macromolecules* **2010**, *43*, 4230−4239.

(10) Thellen, C.; Schirmer, S.; Ratto, J. A.; Finnigan, B.; Schmidt, D. Co-Extrusion of Multilayer Poly(*m*-Xylylene Adipimide) Nanocomposite Films for High Oxygen Barrier Packaging Applications. *J. Membr. Sci.* **2009**, *340*, 45−51.

(11) Ophir, A.; Dotan, A.; Belinsky, I.; Kenig, S. Barrier and Mechanical Properties of Nanocomposites Based on Polymer Blends and Organoclays. *J. Appl. Polym. Sci.* **2010**, *116*, 72−83.

(12) Zhang, S.; Feng, X.; Zhu, S.; Huan, Q.; Han, K.; Ma, Y.; Yu, M. Novel Toughening Mechanism for Polylactic Acid (PLA)/Starch Blends with Layer-Like Microstructure via Pressure-Induced Flow (PIF) Processing. *Mater. Lett.* **2013**, *98*, 238−241.

(13) Priolo, M. A.; Gamboa, D.; Holder, K. M.; Grunlan, J. C. Super Gas Barrier of Transparent Polymer-Clay Multi layer Ultrathin Films. *Nano Lett.* **2010**, *10*, 4970−4974.

(14) Svagan, A. J.; Akesson, A.; Cardenas, M.; Bulut, S.; Knudsen, J. C.; Risbo, J.; Plackett, D. Transparent Films Based on PLA and Montmorillonite with Tunable Oxygen Barrier Properties. *Biomacromolecules* **2012**, *13*, 397−405.

(15) Walther, A.; Bjurhager, I.; Malho, J. M.; Pere, J.; Ruokolainen, J.; Berglund, L. A.; Ikkala, O. Large-Area, Lightweight and Thick Biomimetic Composites with Superior Material Properties via Fast, Economic, and Green Pathways. *Nano Lett.* **2010**, *10*, 2742−2748.

(16) Walther, A.; Bjurhager, I.; Malho, J. M.; Ruokolainen, J.; Berglund, L.; Ikkala, O. Supramolecular Control of Stiffness and Strength in Lightweight High-Performance Nacre-Mimetic Paper with Fire-Shielding Properties. *Angew. Chem., Int. Ed.* **2010**, *49*, 6448−6453.

(17) Ebina, T.; Mizukami, F. Flexible Transparent Clay Films with Heat-Resistant and High Gas-Barrier Properties. *Adv. Mater.* **2007**, *19*, 2450−2453.

(18) Tetsuka, H.; Ebina, T.; Nanjo, H.; Mizukami, F. Highly Transparent Flexible Clay Films Modified with Organic Polymer: Structural Characterization and Intercalation Properties. *J. Mater. Chem.* **2007**, *17*, 3545−3550.

(19) Munch, E.; Launey, M. E.; Alsem, D. H.; Saiz, E.; Tomsia, A. P.; Ritchie, R. O. Tough, Bio-Inspired Hybrid Materials. *Science* **2008**, *322*, 1516−1520.

(20) Deville, S.; Saiz, E.; Nalla, R. K.; Tomsia, A. P. Freezing as a Path to Build Complex Composites. *Science* **2006**, *311*, 515−518.

(21) Lin, T.; Huang, W.; Jun, I.; Jiang, P. Bioinspired Assembly of Colloidal Nanoplatelets by Electric Field. *Chem. Mater.* **2009**, *21*, 2039−2044.

(22) Sellinger, A.; Weiss, P. M.; Nguyen, A.; Lu, Y.; Assink, R. A.; Gong, W.; Brinker, C. J. Continuous Self-Assembly of Organic-Inorganic Nanocomposite Coatings that Mimic Nacre. *Nature* **1998**, *394*, 256−260.

(23) Kochumalayil, J. J.; Bergenstråhle-Wohlert, M.; Utsel, S.; Wågberg, L.; Zhou, Q.; Berglund, L. A. Bioinspired and Highly Oriented Clay Nanocomposites with a Xyloglucan Biopolymer Matrix: Extending the Range of Mechanical and Barrier Properties. *Biomacromolecules* **2012**, *14*, 84−91.

(24) Minelli, M.; Baschetti, M. G.; Doghieri, F. Analysis of Modeling Results for Barrier Properties in Ordered Nanocomposite Systems. *J. Membr. Sci.* **2009**, *327*, 208−215.

(25) Choudalakis, G.; Gotsis, A. D. Permeability of Polymer/Clay Nanocomposites: A Review. *Eur. Polym. J.* **2009**, *45*, 967−984.

(26) Ozcelik, B.; Sonat, I. Warpage and Structural Analysis of Thin Shell Plastic in the Plastic Injection Molding. *Mater. Des.* **2009**, *30*, 367−375.

(27) Jiang, K.; Yu, F.; Su, R.; Yang, J.; Zhou, T.; Gao, J.; Deng, H.; Wang, K.; Zhang, Q.; Chen, F.; Fu, Q. High Speed Injection Molding of High Density Polyethylene: Effects of Injection Speed on Structure and Properties. *Chin. J. Polym. Sci.* **2011**, *29*, 456−464.

(28) Jiang, K.; Yu, F.; Bai, H.; Gao, J.; Deng, H.; Zhang, Q.; Fu, Q. Alternating Multilayer Structure of Polyethylene/Polypropylene

DOI: 10.1021/acsami.5b00347
ACS Appl. Mater. Interfaces 2015, 7, 10178−10189

Blends Obtained through Injection Molding. *J. Appl. Polym. Sci.* **2012**, *124*, 4452−4456.
(29) Na, B.; Wang, K.; Zhang, Q.; Du, R.; Fu, Q. Tensile Properties in the Oriented Blends of High-Density Polyethylene and Isotactic Polypropylene Obtained by Dynamic Packing Injection Molding. *Polymer* **2005**, *46*, 3190−3198.
(30) Zou, F.; Dong, X.; Lin, D.; Liu, W.; Wang, D.; Han, C. C. Morphological and Rheological Responses to the Transient and Steady Shear Flow for a Phase-Separated Polybutadiene/Polyisoprene Blend. *Polymer* **2012**, *53*, 4818−4826.
(31) Akira, O. Phase Transitions of Fluids in Shear Flow. *J. Phys.: Condens. Matter.* **1997**, *9*, 6119−6157.
(32) Han, C. C.; Yao, Y.; Zhang, R.; Hobbie, E. K. Effect of Shear Flow on Multi-Component Polymer Mixtures. *Polymer* **2006**, *47*, 3271−3286.
(33) Jeon, H. S.; Nakatani, A. I.; Hobbie, E. K.; Han, C. C. Phase Inversion of Polybutadiene/Polyisoprene Blends under Quiescent and Shear Conditions. *Langmuir* **2001**, *17*, 3087−3095.
(34) Yu, F.; Deng, H.; Zhang, Q.; Wang, K.; Zhang, C.; Chen, F.; Fu, Q. Anisotropic Multilayer Conductive Networks in Carbon Nanotubes Filled Polyethylene/Polypropylene Blends Obtained through High Speed Thin Wall Injection Molding. *Polymer* **2013**, *54*, 6425−6436.
(35) Grizzuti, N.; Buonocore, G.; Iorio, G. Viscous Behavior and Mixing Rules for an Immiscible Model Polymer Blend. *J. Rheol.* **2000**, *44*, 149−164.
(36) Rezanavaz, R.; Razavi Aghjeh, M. K.; Babaluo, A. A. Rheology, Morphology, and Thermal Behavior of HDPE/Clay Nanocomposites. *Polym. Compos.* **2010**, *31*, 1028−1036.
(37) Hotta, S.; Paul, D. R. Nanocomposites Formed from Linear Low Density Polyethylene and Organoclays. *Polymer* **2004**, *45*, 7639−7654.
(38) Gramespacher, H.; Meissner, J. Melt Elongation and Recovery of Polymer Blends, Morphology, and Influence of Interfacial Tension. *J. Rheol.* **1997**, *41*, 27−44.
(39) Liu, F.; Guo, C.; Wu, X.; Qian, X.; Liu, H.; Zhang, J. Morphological Comparison of Isotactic Polypropylene Parts Prepared by Micro-Injection Molding and Conventional Injection Molding. *Polym. Adv. Technol.* **2012**, *23*, 686−694.
(40) Durmus, A.; Woo, M.; Kasgoez, A.; Macosko, C. W.; Tsapatsis, M. Intercalated Linear Low Density Polyethylene (LLDPE)/Clay Nanocomposites Prepared with Oxidized Polyethylene as a New Type Compatibilizer: Structural, Mechanical and Barrier Properties. *Eur. Polym. J.* **2007**, *43*, 3737−3749.
(41) Arunvisut, S.; Phummanee, S.; Somwangthanaroj, A. Effect of Clay on Mechanical and Gas Barrier Properties of Blown Film LDPE/Clay Nanocomposites. *J. Appl. Polym. Sci.* **2007**, *106*, 2210−2217.
(42) Xu, Y.; Fang, Z.; Tong, L. On Promoting Intercalation and Exfoliation of Bentonite in High-Density Polyethylene by Grafting Acrylic Acid. *J. Appl. Polym. Sci.* **2005**, *96*, 2429−2434.
(43) Wu, D.; Zhang, Y.; Zhang, M.; Yu, W. Selective Localization of Multiwalled Carbon Nanotubes in Poly(ε-Caprolactone)/Polylactide Blend. *Biomacromolecules* **2009**, *10*, 417−424.
(44) Ji, M.; Deng, H.; Yan, D.; Li, X.; Duan, L.; Fu, Q. Selective Localization of Multi-Walled Carbon Nanotubes in Thermoplastic Elastomer Blends: An Effective Method for Tunable Resistivity−Strain Sensing Behavior. *Compos. Sci. Technol.* **2014**, *92*, 16−26.
(45) Yousfi, M.; Soulestin, J.; Vergnes, B.; Lacrampe, M. F.; Krawczak, P. Compatibilization of Immiscible Polymer Blends by Organoclay: Effect of Nanofiller or Organo-Modifier? *Macromol. Mater. Eng.* **2013**, *298*, 757−770.
(46) Gopakumar, T. G.; Lee, J. A.; Kontopoulou, M.; Parent, J. S. Influence of Clay Exfoliation on the Physical Properties of Montmorillonite/Polyethylene Composites. *Polymer* **2002**, *43*, 5483−5491.
(47) Chen, H. M.; Chen, J. W.; Chen, J.; Yang, J. H.; Huang, T.; Zhang, N.; Wang, Y. Effect of Organic Montmorillonite on Cold Crystallization and Hydrolytic Degradation of Poly(L-Lactide). *Polym. Degrad. Stab.* **2012**, *97*, 2273−2283.
(48) Perez, C. J.; Alvarez, V. A. Overall Crystallization Behavior of Polypropylene-Clay Nanocomposites; Effect of Clay Content and Polymer/Clay Compatibility on the Bulk Crystallization and Spherulitic Growth. *J. Appl. Polym. Sci.* **2009**, *114*, 3248−3260.
(49) Yuan, Q.; Awate, S.; Misra, R. D. K. Nonisothermal Crystallization Behavior of Melt-Intercalated Polyethylene-Clay Nanocomposites. *J. Appl. Polym. Sci.* **2006**, *102*, 3809−3818.
(50) Wu, G.; Asai, S.; Sumita, M.; Yui, H. Entropy Penalty-Induced Self-Assembly in Carbon Black or Carbon Fiber Filled Polymer Blends. *Macromolecules* **2002**, *35*, 945−951.
(51) Gao, X.; Zhang, S.; Mai, F.; Lin, L.; Deng, Y.; Deng, H.; Fu, Q. Preparation of High Performance Conductive Polymer Fibres from Double Percolated Structure. *J. Mater. Chem.* **2011**, *21*, 6401−6408.
(52) Wang, K.; Zhao, P.; Yang, H.; Liang, S.; Zhang, Q.; Du, R.; Fu, Q.; Yu, Z.; Chen, E. Unique Clay Orientation in the Injection-Molded Bar of Isotactic Polypropylene/Clay Nanocomposite. *Polymer* **2006**, *47*, 7103−7110.
(53) Kojima, Y.; Usuki, A.; Kawasumi, M.; Okada, A.; Kurauchi, T.; Kamigaito, O.; Kaji, K. Novel Preferred Orientation in Injection-Molded Nylon 6-Clay Hybrid. *J. Polym. Sci., Part B: Polym. Phys.* **1995**, *33*, 1039−1045.
(54) Fan, Y.; Lu, Y. C.; Lu, Y.; Zhang, X.; Lou, J.; Tang, C.; Wood, J. T.; Shinozaki, D. M. Orientation Effect of Clay Platelets in Transfer Molded Polymer Nanocomposites. *Polym.-Plast. Technol. Eng.* **2013**, *52*, 964−973.
(55) Deng, H.; Bilotti, E.; Zhang, R.; Peijs, T. Effective Reinforcement of Carbon Nanotubes in Polypropylene Matrices. *J. Appl. Polym. Sci.* **2010**, *118*, 30−41.
(56) Arora, A.; Choudhary, V.; Sharma, D. K. Effect of Clay Content and Clay/Surfactant on the Mechanical, Thermal and Barrier Properties of Polystyrene/Organoclay Nanocomposites. *J. Polym. Res.* **2011**, *18*, 843−857.
(57) Dong, Y.; Bhattacharyya, D. Effects of Clay Type, Clay/Compatibiliser Content and Matrix Viscosity on the Mechanical Properties of Polypropylene/Organoclay Nanocomposites. *Composites, Part A* **2008**, *39*, 1177−1191.
(58) Delpouve, N.; Stoclet, G.; Saiter, A.; Dargent, E.; Marais, S. Water Barrier Properties in Biaxially Drawn Poly(Lactic Acid) Films. *J. Phys. Chem. B* **2012**, *116*, 4615−4625.
(59) Chatterjee, T.; Patel, R.; Garnett, J.; Paradkar, R.; Ge, S. R.; Liu, L. Z.; Forziati, K. T.; Shah, N. Machine Direction Orientation of High Density Polyethylene (HDPE): Barrier and Optical Properties. *Polymer* **2014**, *55*, 4102−4115.
(60) Liu, R. Y. F.; Schiraldi, D. A.; Hiltner, A.; Baer, E. Oxygen-Barrier Properties of Cold-Drawn Polyesters. *J. Polym. Sci., Part B: Polym. Phys.* **2002**, *40*, 862−877.
(61) Orchard, G. A. J.; Spiby, P.; Ward, I. M. Oxygen and Water-Vapor Diffusion through Biaxially Oriented Poly(Ethylene Terephthalate). *J. Polym. Sci., Part B: Polym. Phys.* **1990**, *28*, 603−621.
(62) Khalili, S.; Masoomi, M.; Bagheri, R. The Effect of Organo-Modified Montmorillonite on Mechanical and Barrier Properties of Linear Low-Density Polyethylene/ Low-Density Polyethylene Blend Films. *J. Plast. Film Sheeting* **2012**, *29*, 39−55.
(63) Ali Dadfar, S. M.; Alemzadeh, I.; Reza Dadfar, S. M.; Vosoughi, M. Studies on the Oxygen Barrier and Mechanical Properties of Low Density Polyethylene/Organoclay Nanocomposite Films in the Presence of Ethylene Vinyl Acetate Copolymer as a New Type of Compatibilizer. *Mater. Des.* **2011**, *32*, 1806−1813.
(64) Jacquelot, E.; Espuche, E.; Gérard, J. F.; Duchet, J.; Mazabraud, P. Morphology and Gas Barrier Properties of Polyethylene-Based Nanocomposites. *J. Polym. Sci., Part B: Polym. Phys.* **2006**, *44*, 431−440.
(65) Sharif-Pakdaman, A.; Morshedian, J.; Jahani, Y. Influence of the Silane Grafting of Polyethylene on The Morphology, Barrier, Thermal, and Rheological Properties of High-Density Polyethylene/Organoclay Nanocomposites. *J. Appl. Polym. Sci.* **2012**, *125*, E305−E313.
(66) Hu, Y. S.; Liu, R. Y. F.; Rogunova, M.; Schiraldi, D. A.; Nazarenko, S.; Hiltner, A.; Baer, E. Oxygen-Barrier Properties of Cold-Crystallized and Melt-Crystallized Poly(Ethylene Terephthalate-co-4,4′-Bibenzoate). *J. Polym. Sci., Part B: Polym. Phys.* **2002**, *40*, 2489−2503.

DOI: 10.1021/acsami.5b00347
ACS Appl. Mater. Interfaces 2015, 7, 10178−10189

(67) Lin, J.; Shenogin, S.; Nazarenko, S. Oxygen Solubility and Specific Volume of Rigid Amorphous Fraction in Semicrystalline Poly(Ethylene Terephthalate). *Polymer* **2002**, *43*, 4733−4743.
(68) Drieskens, M.; Peeters, R.; Mullens, J.; Franco, D.; Lemstra, P. J.; Hristova-Bogaerds, D. G. Structure versus Properties Relationship of Poly(Lactic Acid). I. Effect of Crystallinity on Barrier Properties. *J. Polym. Sci., Part B: Polym. Phys.* **2009**, *47*, 2247−2258.
(69) Zhao, J.; Morgan, A. B.; Harris, J. D. Rheological Characterization of Polystyrene−Clay Nanocomposites to Compare the Degree of Exfoliation and Dispersion. *Polymer* **2005**, *46*, 8641−8660.
(70) Jeon, H. S.; Rameshwaram, J. K.; Kim, G.; Weinkauf, D. H. Characterization of Polyisoprene−Clay Nanocomposites Prepared by Solution Blending. *Polymer* **2003**, *44*, 5749−5758.

DOI: 10.1021/acsami.5b00347
ACS Appl. Mater. Interfaces 2015, 7, 10178−10189